79-4043

Shock Structure in Transonic Compressor Rotors

A. H. Epstein,* J. L. Kerrebrock,† and W. T. Thompkins Jr.‡
Massachusetts Institute of Technology, Cambridge, Mass.

It is argued from a simple model that the radial disequilibrium produced by the jump conditions across the passage shocks in transonic compressor rotors can lead to a stronger shock near the sonic radius than would be predicted by an axisymmetric theory, and to gradients of shock strength, which in turn produce large radial pressure gradients. These pressure gradients lead to strong radial flows in the boundary layer downstream of the shock termination. Shock behavior consistent with the model has been quantified by gas fluorescence measurements in the M.I.T. blowdown compressor; consistent boundary-layer behavior is also observed. Three-dimensional transonic flow computations for the same rotor show radial variations of shock strengths consistent with those from the fluorescent density measurements. It is argued that the described phenomenon can represent an important source of losses. Originating near the transonic radius, the losses appear in the rotor outflow at a larger radius, about midway between the streamtube through the sonic radius and the tip streamtube for the rotor studied. The effect is minimized by designing for a small rate of change of rotor relative Mach number in the radial direction at the sonic radius.

Introduction

THE structure of the shock system in a transonic compressor rotor plays a major role in determining both the radial work distribution and the losses. In axisymmetric design systems an attempt is made to model these effects by shocks satisfying the local normal shock jump conditions on each axisymmetric streamsurface. This leads to estimates for blade chordwise loading distribution and losses that can be incorporated into the streamline-curvature or maxtrix-throughflow computation. Our purpose is first to show by a combination of simple qualitative modeling, flow visualization, and three-dimensional computations that this approach can seriously misrepresent the shock structure and lead to an underestimate of the shock losses, and then to propose a more accurate model for the flow near the sonic radius.

The data that will be presented in support of the proposed model were obtained in the M.I.T. blowdown compressor facility by a technique of fluorescent density measurement,[1] in a rotor with tip Mach number of 1.2 and stagnation pressure ratio near 1.6. Three-dimensional flow computations which display the effects under discussion, have been performed for the same rotor.[2]

We believe that the effect to be described should be present to a significant extent in any transonic high-work rotor. Quantitative analysis of the shock structure will require a fully three-dimensional computation with somewhat greater spatial resolution than has been achieved to date. Additional quantitative measurements by gas fluorescence or by laser velocimetry are also needed to clarify the shock-boundary layer interaction, but we hope the discussion presented here will be helpful in focusing attention on a flow phenomenon of some importance in transonic compressors.

Inadequacy of Axisymmetric Theory

A simple model will suffice to show the major consequences of the axisymmetric assumption at the transonic radius. As indicated in Fig. 1, the relative inflow at velocity V_1' and angle β_1' is assumed aligned to the suction surface. A normal shock reduces the relative velocity to V_2' and changes the pressure from P_1 to P_2. The absolute inflow is assumed axial, so that $V_1' = v_{z1}\sec\beta_1'$ where $\tan\beta_1' = \omega r/v_{z1}$. The axial Mach number, M_{axial}, is taken constant in r.§ In this model P_2/P_1 and V_2'/V_1' are both functions only of $M_1' = V_1'/\sqrt{\gamma RT_1}$, the relative inflow Mach number, and V_2' is aligned with V_1'.

The absolute tangential velocity of the fluid behind the shock is $v_{\theta 2} = \omega r - V_2'\sin\beta_1'$; it then follows that, relative to the rotor, the radial acceleration of a fluid element following the flow is

$$\frac{Dv_{r2}}{Dt} = \frac{v_{\theta 2}^2}{r} - \frac{1}{\rho_2}\frac{dP_2}{dr} = \frac{(\omega r - V_2'\sin\beta_1')^2}{r} - \frac{1}{\rho_2}\frac{dP_2}{dr}$$

In nondimensional form,

$$\frac{r}{a_2^2}\frac{Dv_{r2}}{Dt} = \frac{T_1}{T_2}M_T^2\left(1-\frac{V_2'}{V_1'}\right)^2 - \frac{P_1}{\gamma P_2}\frac{M_T^2}{M_1'}\frac{d(P_2/P_1)}{dM_1'}$$

$$= \left[\frac{T_1}{T_2}\left(1-\frac{V_2'}{V_1'}\right)^2 - \frac{4}{\gamma+1}\frac{P_1}{P_2}\right]M_T^2 \qquad (1)$$

where $M_T^2 = (\omega r)^2/\gamma RT_1$ is the square of the tangential Mach number.

The quantity $(r/a_2^2)Dv_{r2}/Dt$ may be interpreted as half the fractional rate of change of the square of the radial Mach number in distance along the streamtube, the distance being scaled by the radius of the streamsurface. The corresponding upstream quantity $(r/a_1^2)Dv_{r1}/Dt$ is zero; so a jump in the radial acceleration occurs across the shock. The jump is shown at the top of Fig. 2 as a function of radius divided by the tip radius for the values of axial and tangential Mach number characteristic of the M.I.T. blowdown compressor.

It can be seen that the jump in radial acceleration is discontinuous at the sonic radius, where $M_1' = 1$. The value there is just

$$\left.\frac{r}{a_2^2}\frac{Dv_{r2}}{Dt}\right|_{M_1'=1+\epsilon} = -\frac{4}{\gamma+1}M_T^2 \qquad (4)$$

Received April 11, 1978; revision received Nov. 1, 1978.

Index categories: Transonic Flow; Rotating Machinery; Air-breathing Propulsion.

*Research Associate. Member AIAA.

†Maclaurin Professor of Aeronautics and Astronautics. Fellow AIAA.

‡Assistant Professor Aeronautics and Astronautics.

§This assumption will be removed in the detailed comparison with experimental data to follow.

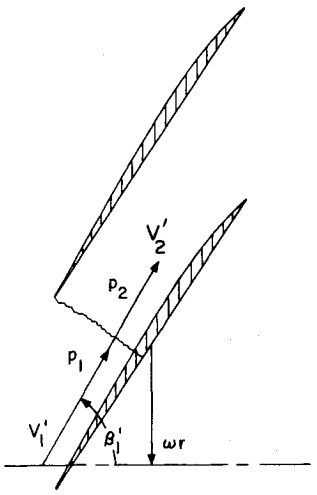

Fig. 1 Schematic of transonic rotor blading, showing notation used in strip theory.

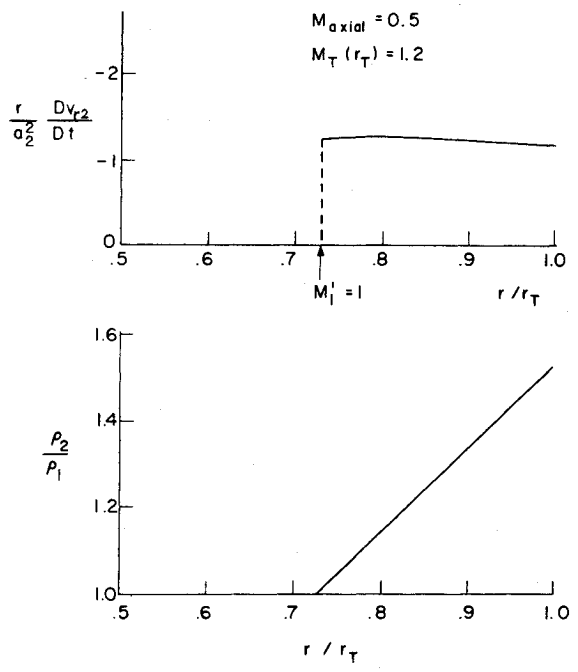

Fig. 2 Density ratio across shock and radial acceleration behind shock which result from strip theory. Note discontinuity in acceleration at $M_1' = 1$.

from which we see that the discontinuity depends directly on the rotor tangential Mach number for this case of zero inlet swirl.

Clearly this discontinuity presents a contradiction, since it attributes to the fluid just outside the sonic radius a strong inward acceleration, while the fluid just inside that radius is not so accelerated. This situation should result in a locally large deviation from the behavior postulated in the axisymmetric model.

In this argument it has been assumed for simplicity that there is no inlet swirl, that the axial Mach number is constant in r, and that the speed of sound a_1 is constant. But Eq. (2) is easily generalized to

$$\left.\frac{r}{a_2^2}\frac{Dv_{r2}}{Dt}\right|_{M_1'=1+\epsilon} = -\frac{4}{\gamma+1}\left(r\frac{dM_1'}{dr}\right)\Bigg|_{M_1'=1+\epsilon} \tag{3}$$

where it has been assumed that $dP_1/dr = 0$. It follows that the disruption of radial equilibrium will occur whenever the relative Mach number passes through unity with a nonzero rate of change in r.

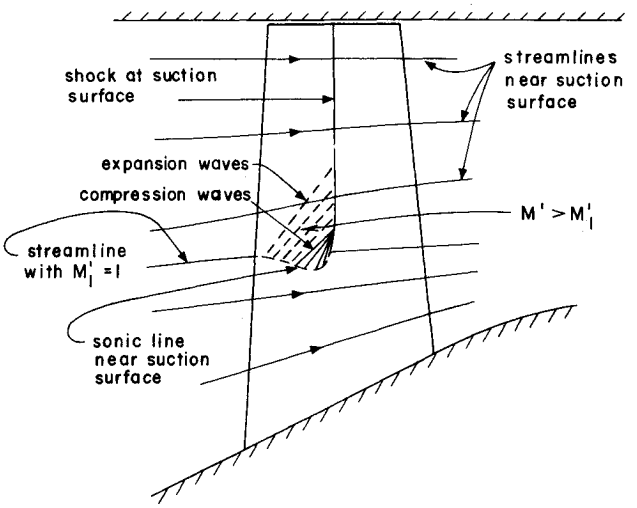

Fig. 3 Schematic of streamline behavior near suction surface, which results from shock termination phenomenon.

Qualitatively, the effect will be to raise the pressure downstream of the shock near its termination at the sonic radius, with consequences that differ greatly in the inviscid flow and in the blade boundary layer. Such an increased pressure can be met by the inviscid flow only if the flow upstream of the shock is expanded to a higher relative Mach number than it would have in the axisymmetric approximation. Thus, we expect an expansion of the streamtubes upstream of the shock near the sonic radius and a corresponding contraction at other radii, as shown schematically in Fig. 3. Because the pressure and Mach number are very sensitive to streamtube area near the sonic point, i.e., proportional to $[1/(1-M^2)]dA/A$, only very slight streamline shifts (on the order of 1% in area) are required to effect the necessary pressure changes. The shifts in Fig. 3 are greatly exaggerated for clarity.

In the region near the shock termination, the flow would first be accelerated through an expansion fan, then compressed through compression waves that coalesce and steepen to form the shock. Figure 3 shows this schematically on a surface parallel to the blade surface. In fact the phenomenon is highly three dimensional, the shock surface curving upward toward the tip and toward the pressure surface so as to focus the expansion and compression waves near the shock termination on the suction surface.

The boundary-layer fluid approaching the shock near its termination will feel not only a very strong adverse streamwise pressure gradient, but also a very large radial pressure gradient due to the jump condition at the sonic radius. From the preceding arguments the radial dynamic pressure developed in the boundary layer should be, from Eq. (2), of the order

$$\Delta M_r^2 \simeq 2\frac{\Delta\ell}{r}\frac{4}{\gamma+1}(1-M_{axial}^2)$$

where $\Delta\ell$ is the distance along the streamtube over which the radial pressure unbalance operates on the boundary layer fluid. Taking $\Delta\ell$ on the order of half the blade chord and $M_{axial} \simeq 0.5$, we find that for the M.I.T. blowdown compressor

$$\Delta M_r^2 \simeq 2\left(\frac{1.5\text{ in.}}{9\text{ in.}}\right)\frac{4}{2.4}\left(\frac{3}{4}\right) \simeq 0.41 \text{ or } \Delta M_r \simeq 0.65$$

These arguments suggest the possibility of a very strong three-dimensional interaction between the transonic inviscid flow and the boundary layer near the shock termination. In

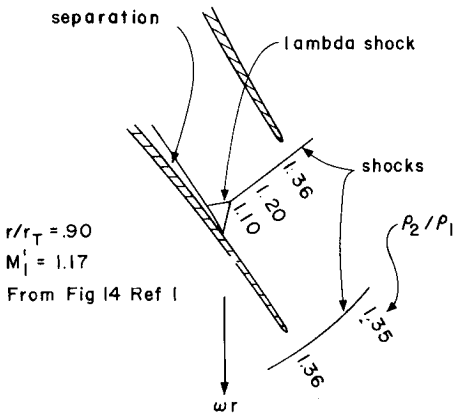

Fig. 4 Density map in rotor passage at $r/r_T = 0.90$, showing lambda shock and boundary layer interaction.

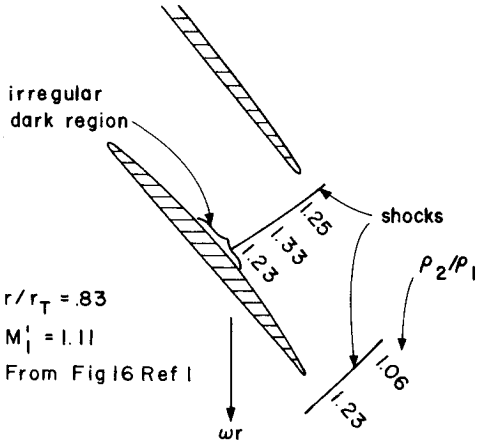

Fig. 5 Density map in rotor passage at $r/r_T = 0.83$ showing relatively weak shock and irregular low density region behind shock at suction surface.

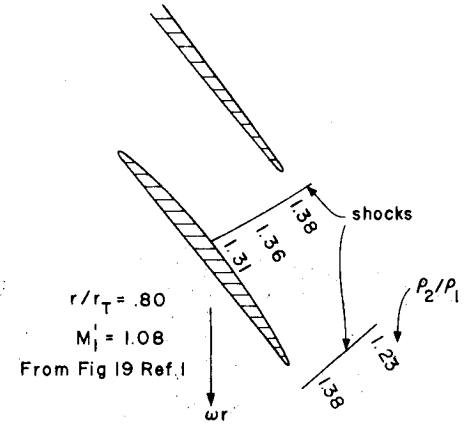

Fig. 6 Density map in rotor passage at $r/r_T = 0.80$ showing shock much stronger than predicted by strip theory and lack of boundary-layer separation.

the following sections experimental and computational evidence that leads to a more complete description of the flow will be described.

Fluorescent Density Measurements

The primary experimental evidence for existence of the shock structure described in the last section is in the quantitative density measurements by gas fluorescence by Epstein. These results were presented in full in Ref. 1. Tracings of three photographs particularly relevant to the present

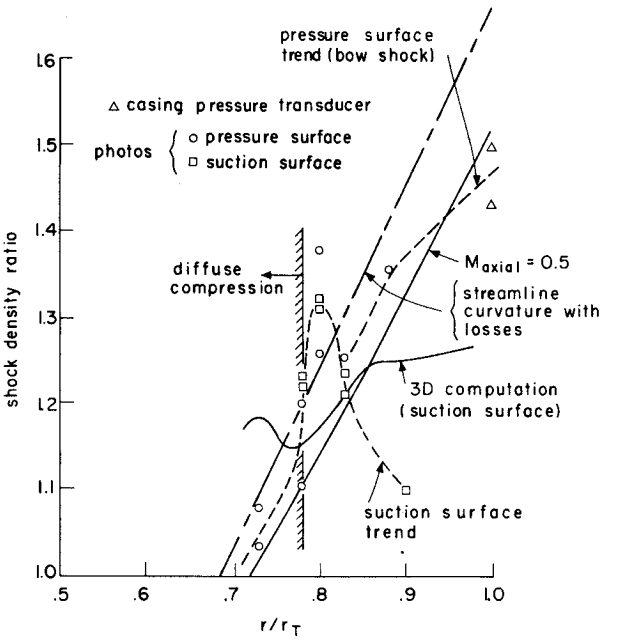

Fig. 7 Comparison of density ratios across shock as predicted by strip theory and by three-dimensional computation, with values from fluorescent density measurements at suction and pressure surfaces. Data from tip pressure transducer are included at $r/r_T = 1.0$.

argument are presented in Figs. 4-6. The original photographs show the intensity of fluorescence of gas illuminated in a plane defined by a very thin sheet of light nearly perpendicular to the blade span. The apparent intensity in the photographs is complicated by variations of excitation, gain in imaging system, and film response, all of which were corrected in Ref. 1 to give quantitative density plots. For the present purposes, the density ratios across the shocks can be inferred directly from the jumps in density of the photographic negatives, appropriate account being taken of film response, and these values are noted along the shocks.

Such results are plotted in Fig. 7 against radius for two points on each shock. The circular points indicate the density ratio for the shock near the pressure surface, that is, essentially for the bow shock, while the square points indicate the shock density ratio near the suction surface. The triangular points at $r/r_T = 1.0$ were obtained from a casing mounted pressure transducer about 0.05 chord upstream of the leading edge; hence they also indicate the pressure surface shock strength. For $r/r_T < 0.8$ there is not a clearly defined shock but rather a steep diffuse compression; the approximate pressure ratio across these compression regions have been plotted for $r/r_T = 0.78$ and 0.73.

The striking feature of these results is the abrupt increase in shock strength at $r/r_T = 0.80$ near both the suction and pressure surfaces. The bow shock strength follows the axisymmetric theory approximately for $r/r_T > 0.83$, but then jumps up to a value of 1.25 to 1.4 at $r/r_T = 0.80$ where the axisymmetric theory would indicate a value of 1.15. There is some variation from photograph to photograph at this radius, as shown in Fig. 7, the source of variation being unknown. It is possible that slight uncertainty in the radial placement of the light plane could contribute to the variation.

Near the suction surface the shock strength varies from about 1.1 at $r/r_T = 0.9$ through a peak of 1.3 at $r/r_T = 0.8$. From Fig. 4 it can be seen that there is a strong shock-boundary layer interaction at $r/r_T = 0.9$, which probably limits the shock strength there. At $r/r_T = 0.83$ (Fig. 5) the shock is of nearly uniform strength across the passage, and an irregular region of very low density is visible just downstream of the shock termination at the suction surface. There is no lambda structure. At $r/r_T = 0.80$ (Fig. 6) the shock is very

strong and appears to terminate at the surface without a lambda shock or other boundary layer phenomena, although it must be noted that the blade twist blocks the surface itself from view in this photograph.

Finally, at $r/r_T = 0.78$, the shock has changed to a steep but diffuse compression. Photographs at smaller radii show that this steep compression propagates almost radially all the way to the hub surface.

Computational Results and Comparison to Experiment

A fully three-dimensional inviscid computation of the flow in this rotor has been carried out by Thompkins.[2] Due to limitations on grid spacing and computational methods, this computation does not give sharp resolution of the shocks, so is not capable of distinguishing the shocks of Figs. 4-6 from the diffuse compression that occurs at small radii. It does seem though that it should represent the inviscid acceleration discontinuity predicted by the strip theory but modified by three-dimensional effects. Shock strengths estimated from the computation near the suction surface are shown in Fig. 7. The sudden increase in density ratio near the sonic radius is exhibited by the computation, although it occurs at a smaller radius than in the experiment. At radii larger than the sonic radius, the three-dimensional computation follows the density ratio at the pressure surface more closely than that at the suction surface. This is consistent with the idea that the actual shock strength at the suction surface is limited by the shock boundary layer interaction, which of course is not included in the computation. Thus, in the computational results, the shock is of nearly uniform strength across the passage.

To put the experimental and computational results into perspective, the predictions of axisymmetric theory have been added to Fig. 7 at two levels of sophistication. The curve labeled "$M_{\text{axial}} = 0.5$" represents the very simple model just described, where the relative Mach number is computed from the rotational Mach number and a uniform axial Mach number, and normal shocks are assumed at this relative Mach number. A second curve, labeled "streamline curvature with losses," again assumes normal shocks at the blade inlet relative Mach number which, however, has been computed by Sehra[3] using a modified version of the streamline curvature program of Ref. 4.¶ This computation includes the effects of measured losses and also the effects of the "apparent stresses" due to blade-to-blade flow variations. It gives quite an accurate prediction of both the axial and the tangential mean velocities at the rotor exit; thus it should represent the axisymmetric theory in an accurate form.

There is a small uncertainty in the relative levels of axial Mach number (weight flow) between the experiment and the three theoretical curves; so the small vertical shifts should be ignored. Apart from this we see that the two approximations of axisymmetric theory give nearly the same result and that they differ from the experimental and three-dimensional computational results in two ways. First, there is the peak at the transonic radius. Second, the experimental and computed shock strength falls off near the tip relative to that predicted by axisymmetric theory. While the origins of this second effect are not entirely clear at present, it can be remarked that the streamline configuration sketched in Fig. 3 does imply a diffusion of the flow near the tip, since the streamlines must contract there to allow for the divergence near the transonic radius.

Loss Mechanisms

There are two possible sources of additional loss due to the shock termination phenomenon. The rapid variations in shock strength produce entropy gradients and corresponding vorticity, and the strong pressure gradients generated in the inviscid flow interact with the boundary layer to produce intense secondary flows. Of the two sources of loss, the second is most important.

To show this, we first estimate the magnitude of the vorticity produced in the inviscid flow by the shock strength variations. By Crocco's theorem, $\Omega \times V' = T\nabla S - \nabla I$. Here Ω is the vorticity, V' the relative velocity, and I the rothalpy, which will be assumed constant. The entropy change across the shock is given by

$$\frac{s_2 - s_1}{R} = \frac{2\gamma}{3(\gamma+1)^2}\left[\frac{\gamma+1}{2\gamma}\left(\frac{P_2}{P_1} + \frac{\gamma-1}{\gamma+1}\right) - 1\right]^3$$

which gives $(s_2 - s_1)/R = 0.0065$ for $P_2/P_1 = 1.4$, and 0.0028 for $P_2/P_1 = 1.3$. In dimensionless form, the entropy gradient between $r/r_T = 0.80$ and 0.83 in Fig. 7 is thus $r_T \nabla s/R \simeq 0.003/0.03 = 0.1$; from Crocco's equation

$$\Omega V' \simeq T\nabla S \simeq (RT/r_T)\,(0.1)$$

or

$$\frac{\Omega r_T}{V'} \simeq \frac{RT}{(V')^2}(0.1) = \frac{0.1}{\gamma M^2} \simeq 0.07$$

Thus, even on the length scale of the tip radius, the vorticity would produce a velocity only 0.07 of the relative velocity. On the length scale of the shock termination region, which is about $0.05\, r_T$, the rotational velocity disturbance due to shock strength variation is very small, less than 1% of the mean relative velocity.

On the other hand, the boundary layer on the suction surface is subjected to the extreme pressure gradients implied by the density variation of Fig. 7, $[P_2/P_1 = (\rho_2/\rho_1)^\gamma]$. Since the flow in the boundary layer is not transonic, the same pressure disturbance will produce much larger spanwise displacements of the streamlines than in the inviscid flow. The result is shown schematically in Fig. 8, where an attempt has been made to depict the development of the boundary layer at several radii. At $r/r_T = 0.90$ (and probably at $r/r_T = 1.0$ also) there is a lambda shock due to separation. At $r/r_T = 0.83$, there does not appear to be separation; rather there is a very strong streamwise vortex, apparently formed by the spanwise flow in the boundary layer away from the pressure peak at $r/r_T = 0.80$. This streamwise vortex is apparent as the irregular region of low density at the juncture of the shock with suction surface in Fig. 5. At $r/r_T = 0.80$ there is again no evidence of separation, and the boundary layer is relatively well behaved downstream of shock impingement.

From the pressure difference between $r/r_T = 0.80$ and $r/r_T = 0.83$, we would expect Mach numbers of the order of 0.4 to 0.6 in the vortex shed at $r/r_T = 0.83$. Concentrated radial and tangential velocity disturbances of this magnitude were found in surveys behind the trailing edge at $r/r_T \simeq 0.86$.[2] A concentration of high entropy fluid also occurs at the same location. It should be noted that the losses traceable to the shock termination phenomenon do not appear in the streamtube passing through the transonic radius, but rather at a larger radius. For the rotor described here the transonic radius is at $r/r_T \simeq 0.7$, while the losses appear in the outflow at $r/r_T \simeq 0.86$.

Generalization and Conclusion

It appears that the strong interaction near the sonic radius that has been identified here should exist to some degree in any transonic rotor unless the relative Mach number upstream of the passage shock system satisfies the constraint given by Eq. (3), that $r\, dM_1'/dr = 0$ at the sonic radius (where $M_1' = 1$). For a rotor with uniform axial Mach number and no preswirl, this implies $M_T = 0$ at $M_1' = 1$. Thus, rotors without inlet guide

¶The authors are indebted to A. A. Mikolajczak for the suggestion that this comparison be included.

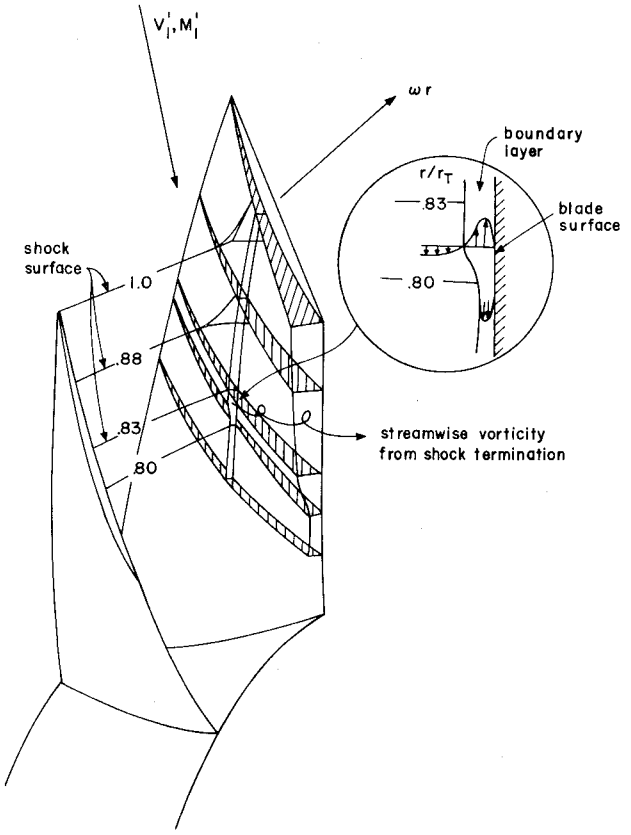

Fig. 8 Schematic of shock structure and boundary layer on suction surface showing mechanism for production of losses by spanwise flow in boundary layer at shock termination.

vanes should exhibit the phenomenon, and it should be more pronounced the larger the value of M_T at which $M_1'=1$. Since for such a rotor $M_T^2=1-M_{\text{axial}}^2$ when $M_1'=1$, the phenomenon should be more noticeable for rotors with lower axial Mach numbers.

The effect of preswirl can be estimated in first approximation by assuming radial equilibrium behind the inlet guide vanes; then the radial variation of axial Mach number is given approximately by

$$M_{\text{axial}}\frac{dM_{\text{axial}}}{dr}=-\frac{M_\theta}{r}\frac{d}{dr}(M_\theta r)$$

Using the fact that $(M_1')^2=M_{\text{axial}}^2+(M_T-M_\theta)^2$, we can then show that

$$r\frac{dM_1'}{dr}\bigg|_{M_1'=1}=M_T^2-(M_T+M_\theta)M_\theta-M_T r\frac{dM_\theta}{dr} \qquad (4)$$

which is consistent with Eqs. (2) and (3) for $M_\theta=0$. The condition that there be no discontinuity in radial acceleration at the sonic radius follows from setting $r(dM_1'/dr)=0$ and is

$$r\frac{dM_\theta}{dr}=M_T-M_\theta-M_\theta^2/M_T \quad (M_1'=1) \qquad (5)$$

This expression is plotted as a function of M_θ for selected values of M_T in Fig. 9. The interpretation of this figure is that for selected values of M_θ and M_T at the sonic radius, the rate of change of M_θ with r must be as given if the discontinuity is to be avoided. Thus, for example, if $M_\theta=0.4$ and $M_T=0.8$ at

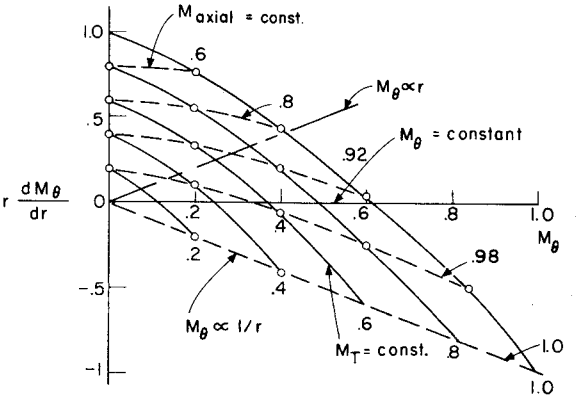

Fig. 9 Representation of inlet swirl Mach number variation required to eliminate the discontinuity at the sonic radius. All values are at $M_1'=1$. Two special cases of solid body rotation ($M_\theta \propto r$) and free vortex ($M_\theta \propto 1/r$) are shown as limits of usual design practice.

the sonic radius, $r dM_\theta/dr=0.2$ is required. The overlay of dashed lines gives M_{axial}, which for this example is $M_{\text{axial}}=0.92$.

Two special types of swirl are shown in Fig. 9. For $M_\theta \propto r$, $r dM_\theta/dr=M_\theta$, and for $M_\theta \propto 1/r$, $r dM_\theta/dr=-M_\theta$. The latter dependence corresponds to $M_\theta=M_T$ at $M_1'=1$; hence $M_{\text{axial}}=1$. This in turn implies zero stagger at the sonic radius.

Most stage designs will lie between the two limits of $M_\theta \propto r$ and $M_\theta \propto 1/r$; so from Fig. 9 we can see that the criterion for no discontinuity at the shock termination is likely to be satisfied only if M_{axial} is quite near to unity. The minimum permissible value of M_{axial} between these limits of swirl variation is 0.8. This occurs for $M_\theta=0.4$, $M_T=1$, and $M_\theta \propto r$. To eliminate the discontinuity at M_{axial} lower than 0.8, a radial variation of swirl more rapid than a solid body rotation would be required.

In this discussion it has been assumed that the Mach number M_1' relative to the blade leading edge is also that entering the shock; i.e., that the inlet flow is aligned to a flat suction surface. Expansion or compression on the suction surface would modify the variation of M_1' in r, but it seems unlikely that it would lead to $r dM_1'/dr=0$ at M_1' except by design intent.

There is reason to doubt whether the shock structure observed in this particular transonic rotor is typical, since the resultant loss region has not been clearly identified in other rotors. It is hoped that further investigation will illuminate this issue.

Acknowledgment

This research was sponsored by NASA Lewis Research Center under Grant NGL 22-009-383.

References

[1] Epstein, A. H., "Quantitative Density Visualization in a Transonic Compressor Rotor," *Journal of Engineering for Power*, Vol. 99, July 1977, pp. 460-475.

[2] Thompkins, Jr., W. T., "An Experimental and Computational Study of the Flow in a Transonic Compressor Rotor," Ph.D. Thesis, Massachusetts Institute of Technology, June 1976; also M.I.T. Gas Turbine Lab. Rept. No. 129, May 1976.

[3] Sehra, A. K., Private communication of results from research supported by Air Force Aero Propulsion Laboratory under Contract No. F33615-76-C-2118; C. H. Law, Technical Monitor.

[4] Hearsey, R. M., "A Revised Computer Program for Axial Compressor Design," ARL TR-75-0001, I&II, Aerospace Research Laboratory, USAF Wright Patterson AFB, Ohio, Jan. 1975.